Supporting Information

Conductive Graphene-Based E-textiles for Highly Sensitive, Breathable, and Water-Resistant Multimodal Gesture-Distinguishable Sensor

Xurui Hu[1,#], Tao Huang[2,#], Zhiduo Liu[3], Gang Wang[1,5,*], Da Chen[1], Qinglei Guo[4], Siwei Yang[2], Zhiwen Jin[6], Jong-Min Lee[5,*], and Guqiao Ding[1,2,*]

[1]Department of Microelectronic Science and Engineering, School of Physical Science and Technology, Ningbo University, Ningbo 315211, P. R. China.

E-mail: gangwang@nbu.edu.cn

[2]State Key Laboratory of Functional Materials for Informatics, Shanghai Institute of Microsystem and Information Technology, Chinese Academy of Sciences, Shanghai 200050, P. R. China.

E-mail: gqding@mail.sim.ac.cn

[3]State Key Laboratory of Integrated Optoelectronics, Institute of Semiconductors, Chinese Academy of Sciences, Beijing 100083, P. R. China.

[4]School of Microelectronics, Shandong University, Jinan 250100, P. R. China.

[5]School of Chemical and Biomedical Engineering, Nanyang Technological University, Singapore.

E-mail: JMLEE@ntu.edu.sg, gangwang@nbu.edu.cn

[6]School of Physical Science and Technology & Key Laboratory for Magnetism and Magnetic Materials (MoE), Lanzhou University, Lanzhou 730000, P. R. China.

[#]X.H. and T.H. contribute equally to this work.

Preparation of graphene: a reaction mixture composed of 1 g graphite, 10 g $Na_2S_2O_8$, and 90 ml sulfuric acid was kept at room temperature for 10 min under constant stirring. Then, the mixture was transferred to a kettle pre-heated to 80 °C and held for 30 min under constant stirring (350 rpm). The product was isolated by filtration, and the filtrated solution was collected for the next graphite exfoliation cycle. After rinsing thoroughly with water and ethanol, the product was dried at 50 °C in ambient air for 5 h to obtain a fluffy powder. This was then dispersed in NMP under 2 hours of ultrasonic treatment to get the 20 mg/ml graphene/NMP slurry.

The reaction process of MTCS-PMS:

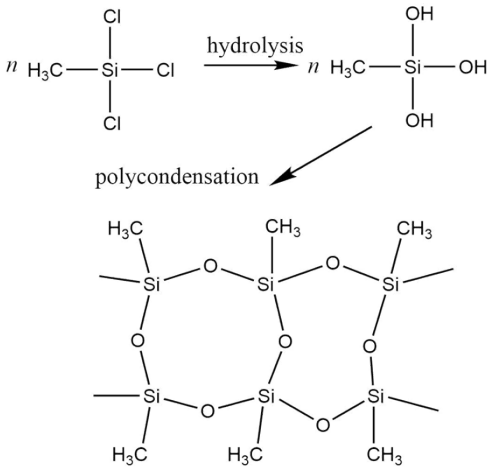

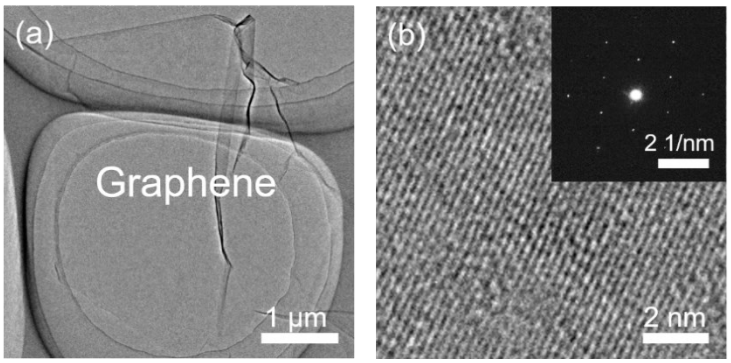

Fig. S1 (a) TEM image of graphene. (b) HR-TEM images showing lattice fringe of graphene, illustration is the selected area electron diffraction pattern of graphene.

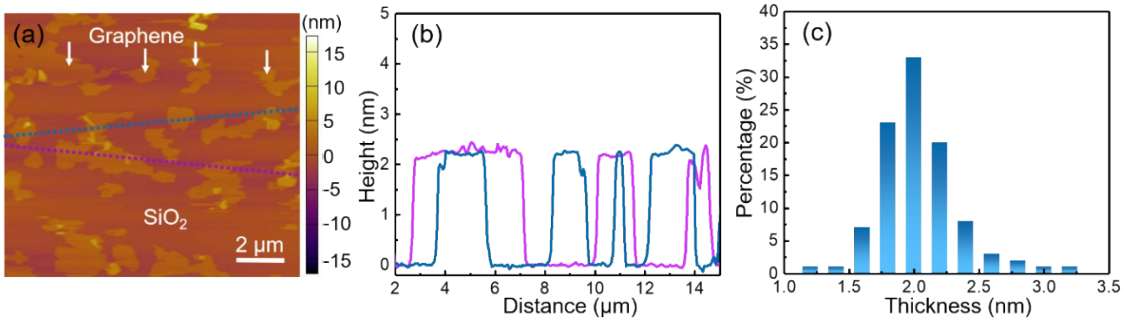

Fig. S2 (a) AFM images of graphene. (b) Thickness profile along the line in (a). (c) Flake thickness distribution of graphene.

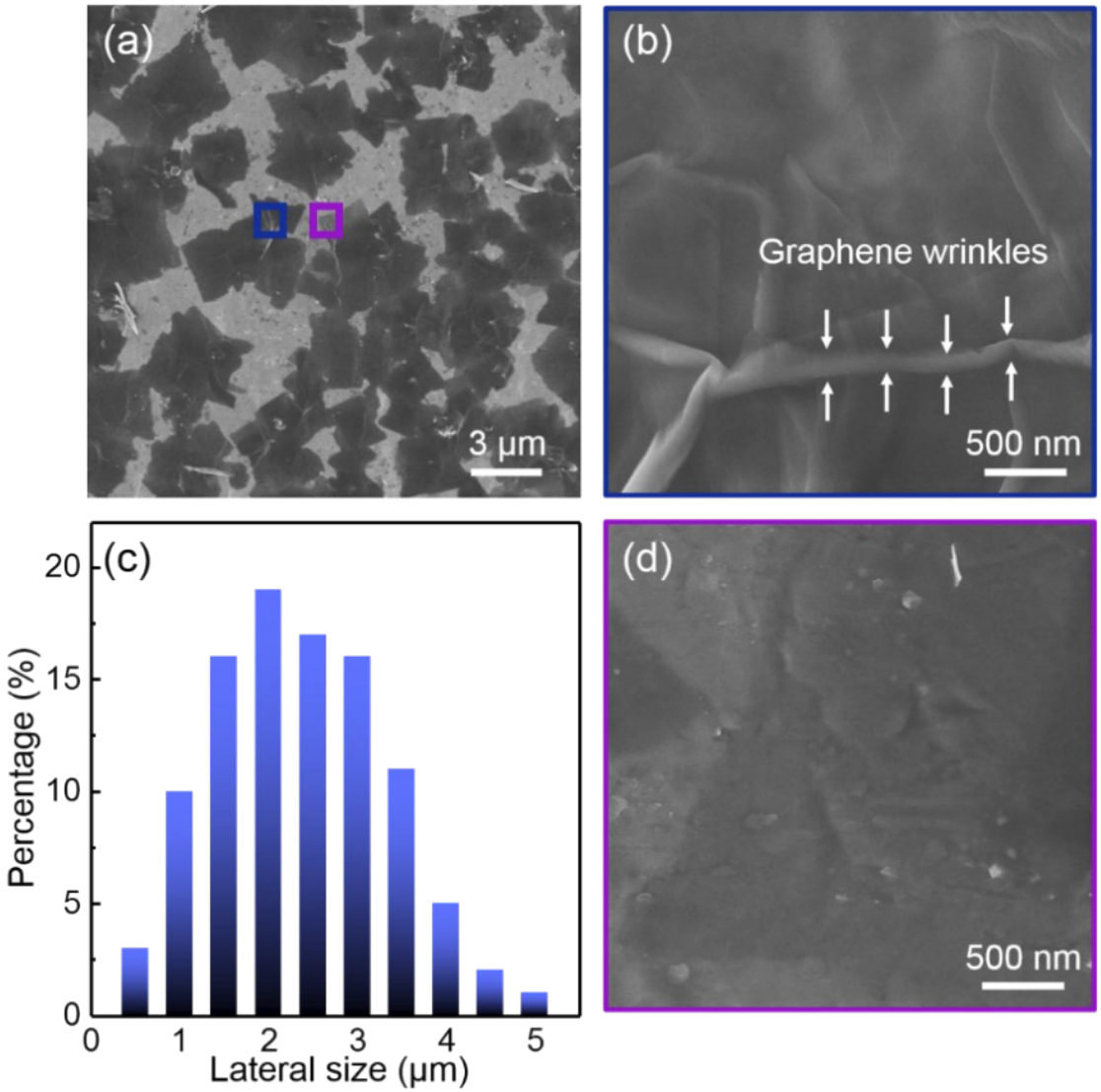

Fig. S3 (a) SEM image of graphene flakes. (b, d) partially magnified image from (a). (c) Flake size distribution of graphene.

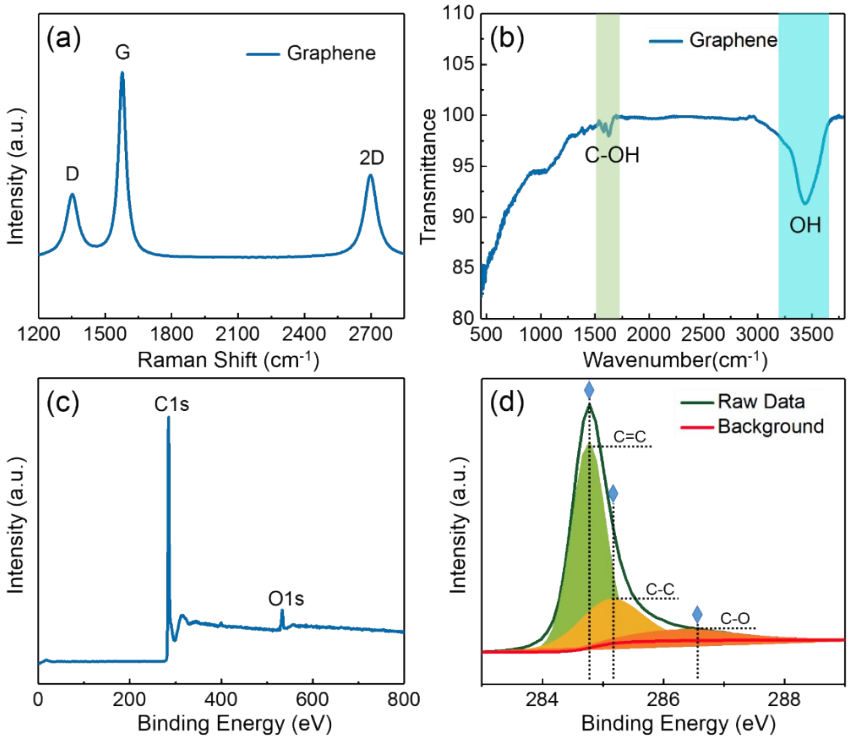

Fig. S4 Raman (a) and FT-IR (b) of graphene, XPS (c, d) results of graphene and C 1s peak analysis are showing the high-quality of graphene and less oxygen groups.

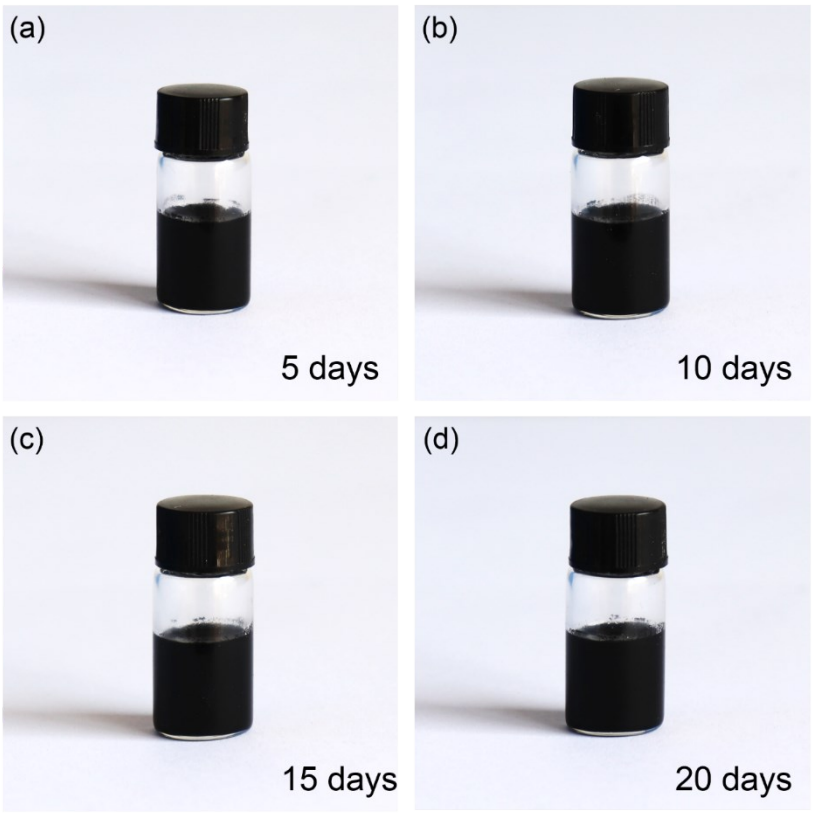

Fig. S5 (a-d) Graphene dye solution standing still for 5-20 days. After 20 days' settling down, no clear delamination or sediment in the solution was observed, indicating excellent dispersibility of graphene.

Regulation of copper content: it is worth mentioning that the optimum Cu content is about 0.4 (weight ratio to the solute) as shown in **Fig. S6 (a)**. With the increase of Cu content to 0.4, the sheet resistance of fabric would drop quickly. After that, more Cu content wouldn't bring a quick drop of resistance. However, if the ratio of Cu is too high (over 1), the graphene-based coatings will be easily brittle and delaminated, which cannot guarantee the integrity and mechanical stability of the device. Compared with the optimum ratio of Cu and graphene, the mechanical treating of graphene-based E-textiles under higher Cu content will result in graphene sheets delaminated, as shown in **Figs. S6 (b-c)**. The magnified SEM image shows the shape and diameter of graphene fiber (the optimum the ratio of Cu and graphene) remain the same after mechanically treated, as shown in **Fig. S6 (d)**, and no coating layer exfoliation was observed. However, under higher Cu content, the shape and diameter of graphene fiber (**Fig. S6 (e)**) showing the presence of micrometer-sized patches. If the ratio of Cu is too low (less than 0.2), the fabric will be not conductive enough, which brings higher demand to the test equipment and decreases the precision of motion distinguishing.

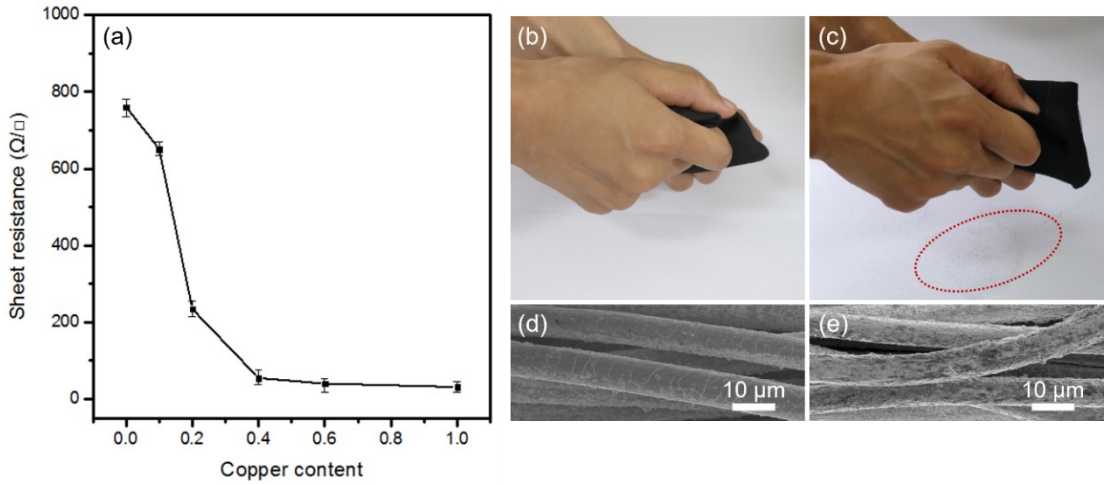

Fig. S6 (a) The sheet resistance of fabric as a function of the ratio of Cu. (b) A real image demonstrating the stability of coatings of graphene-based E-textiles with mechanical treatment under the optimum ratio of Cu and graphene. (c) A real image demonstrating the stability of coatings of graphene-based E-textiles with mechanical treatment under the high the ratio of Cu and graphene. (d) The magnified SEM image of the connection between graphene sheet and fibers with mechanical treatment from a real image (b). (e) The magnified SEM image of the connection between graphene sheet

and fibers with mechanical treatment from a real image (c).

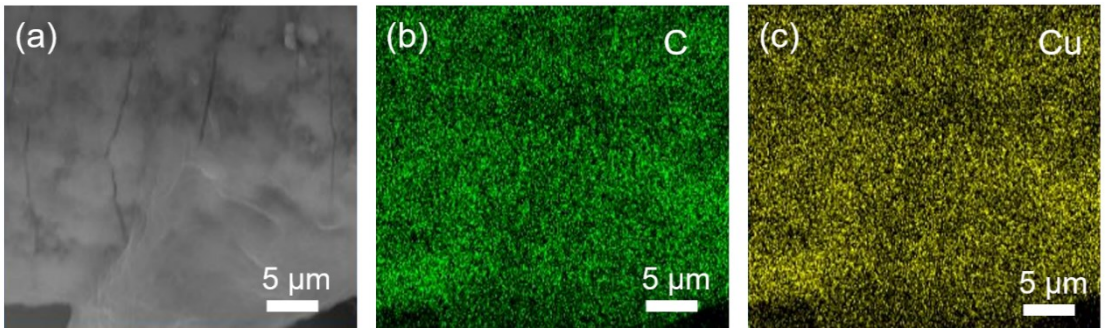

Fig. S7 Uniformity of hybrid Cu particles Functionalized graphene textiles. (a) SEM image of the hybrid architecture. EDS elemental maps of (b) C, and (c) Cu in the hybrid architecture.

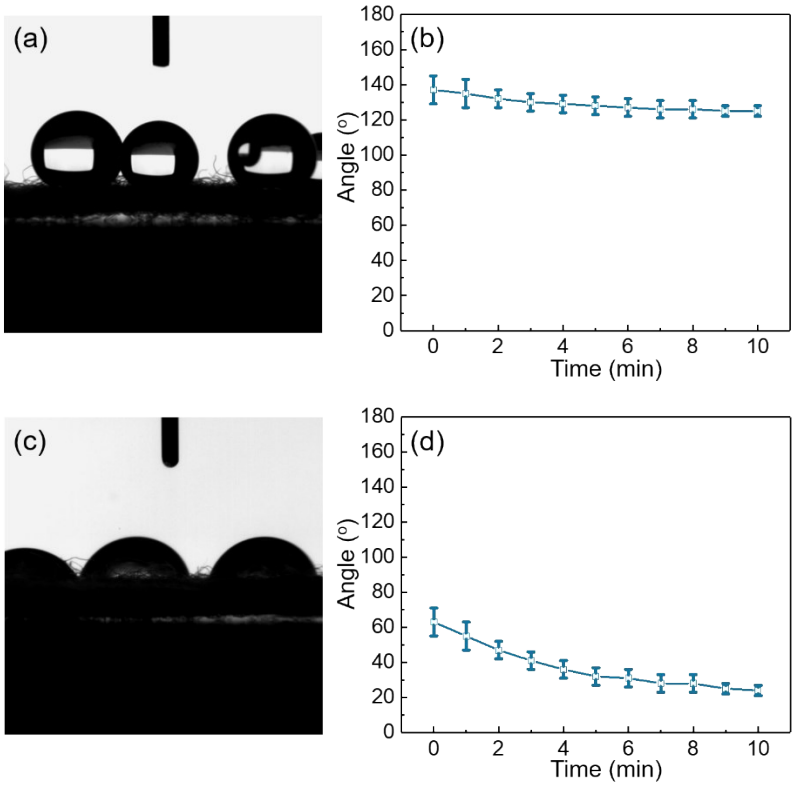

Fig. S8 (a) A plurality of water droplets are continuously dropped on the graphene E-textile. (b) The contact angle change on the graphene E-textile was within 10 minutes. (c) A plurality of water droplets are continuously dropped on the original textile. (d) The contact angle change on the original textile was within 10 minutes.

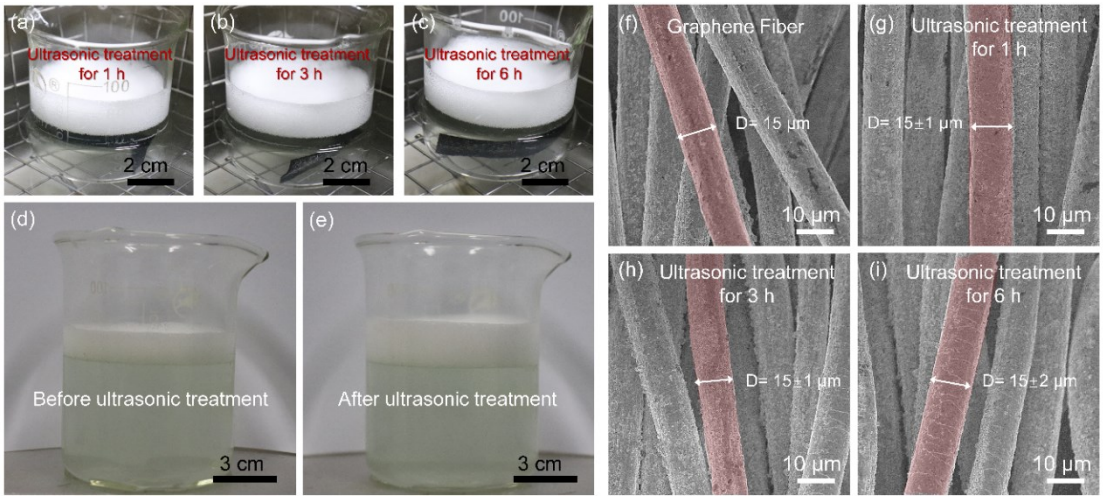

Fig. S9 The graphene-based E-textiles with the ultrasonic washing process. (a) After ultrasonic washing in the detergent for 1 hour, (b) after ultrasonic washing in the detergent for 3 hours, (c) after ultrasonic washing in the detergent for 6 hours. (d and e) Comparing the changes in detergent before and after ultrasonic cleaning. SEM images of the graphene-based E-textiles before ultrasonic washing (f), after 1 hour (g), after 3 hours (h), and after 6 hours (i) of ultrasonic washing.

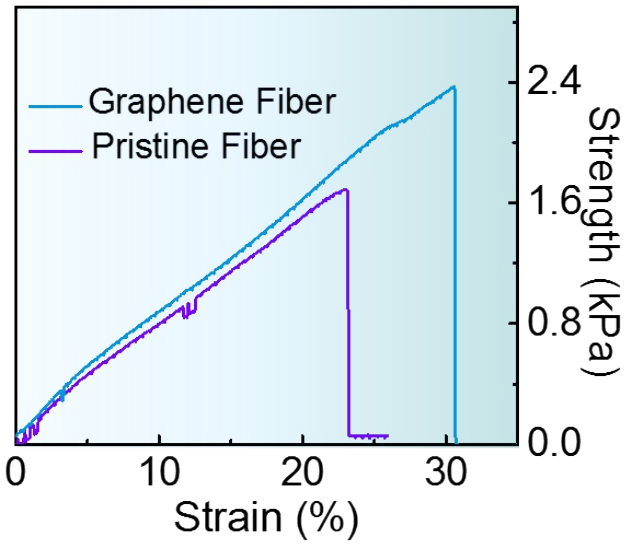

Fig S10. The strength-strain curve of fabric.

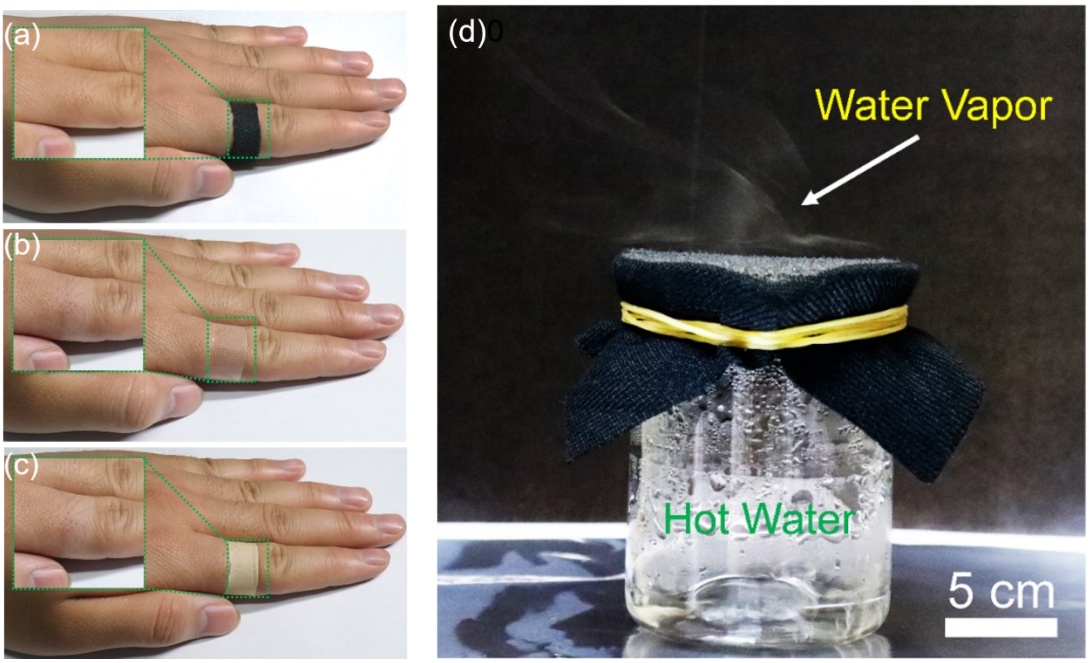

Fig. S11 (a) Graphene-based E-textiles, (b) medical polymer, and (c) the silicone film bundled on the finger for 48 hours to assess wearability and comfort. (d) A real image demonstrating the excellent breathability and air permeability properties of graphene-based E-textiles.

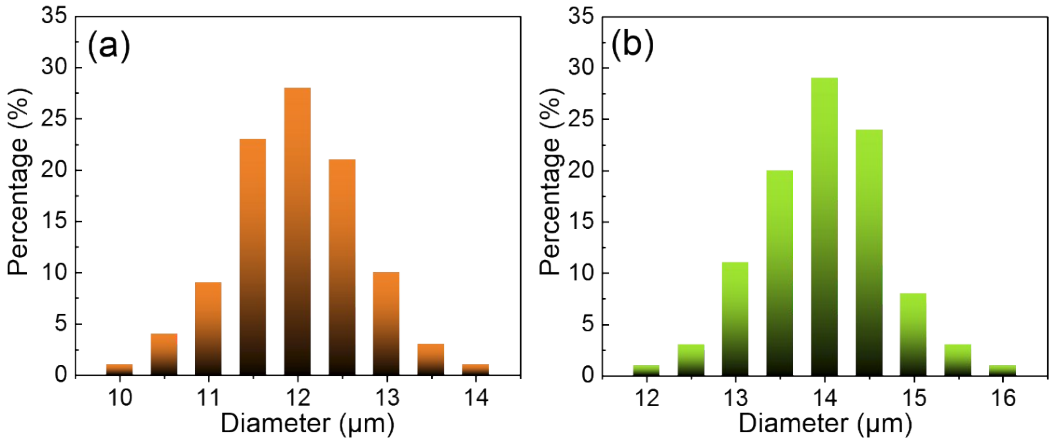

Fig. S12 (a) Diameter distribution of original fabric fibers. (b) Diameter distribution of graphene E-textile fibers.

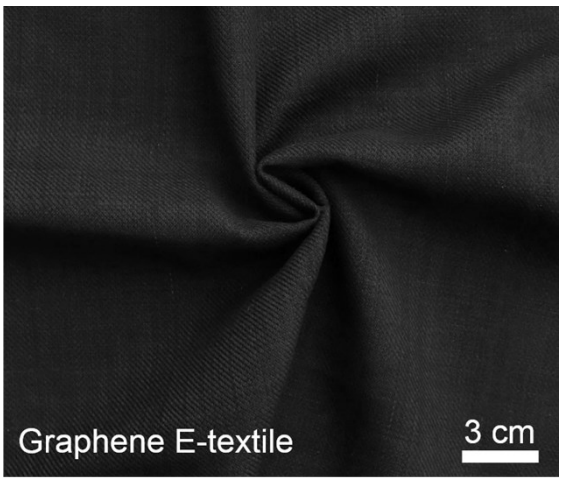

Fig. S13 Optical image of graphene E-textile, the same flexibility as original textiles.

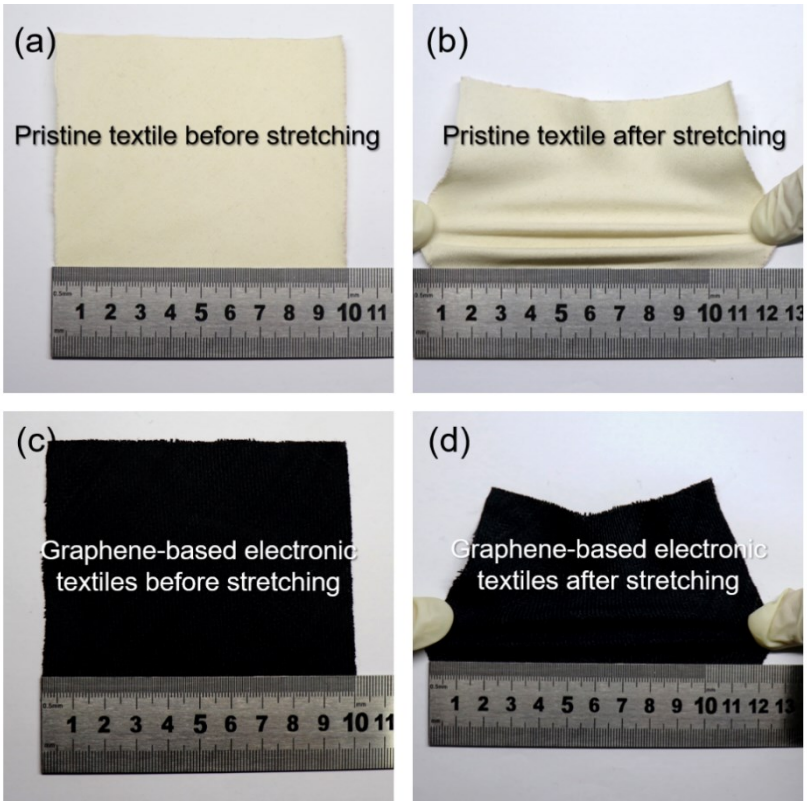

Fig. S14 (a) A real image of the pristine textile before stretching. (b) A real image of the pristine textile after stretching. (c) A real image of the graphene-based E-textiles before stretching. (d) A real image of the graphene-based E-textiles after stretching.

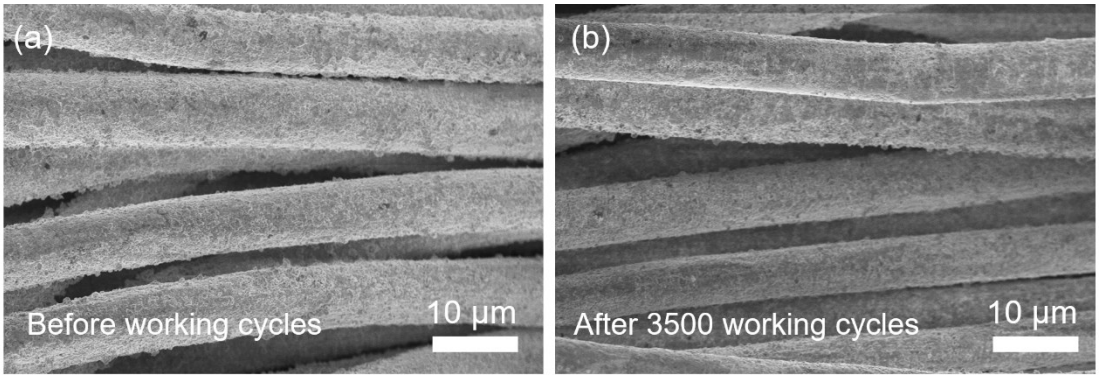

Fig. S15 The magnified SEM images of the shape and diameter of graphene-based E-textiles (a) before and (b) after 3500 working cycles.

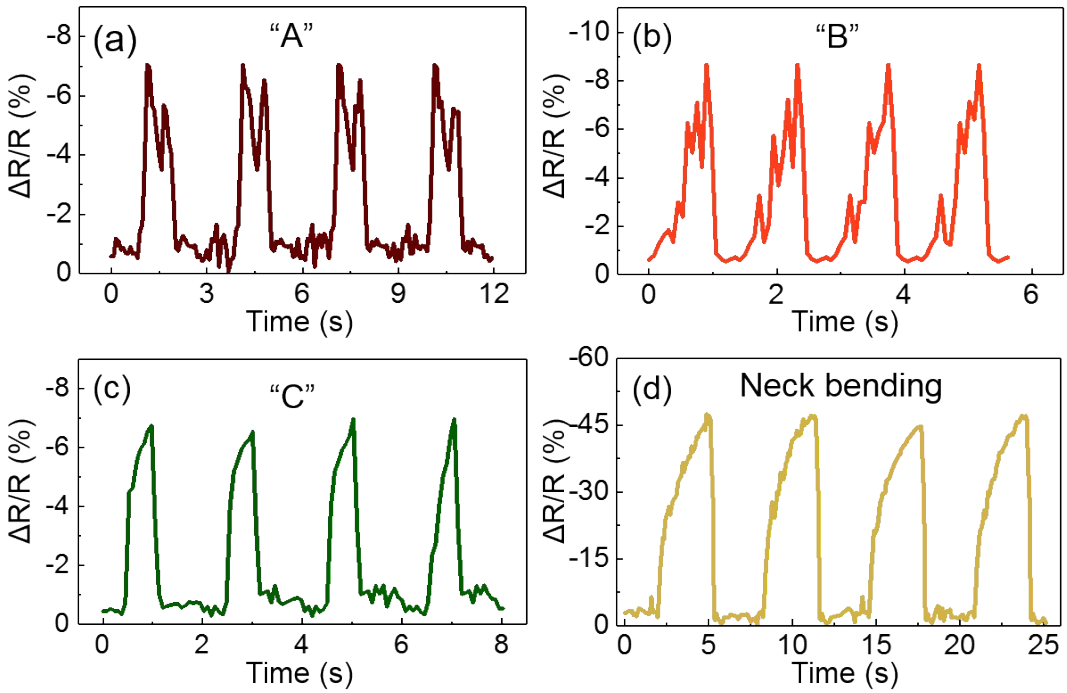

Fig. S16 (a, b and c) The relative resistance changes of the different English alphabets with hand-writing. (d) The relative resistance changes of the neck bending.

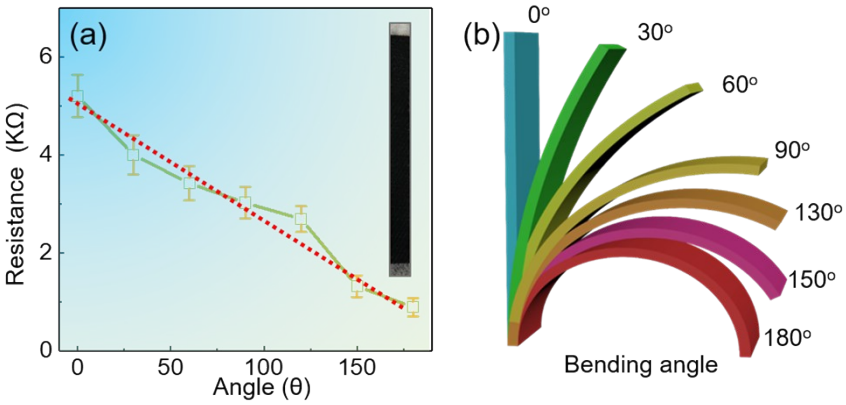

Fig. S17 (a) Graphene E-textile bending sensors change resistance during bending, the illustration shows a bend sensor. (b) A schematic diagram of the bending angle.

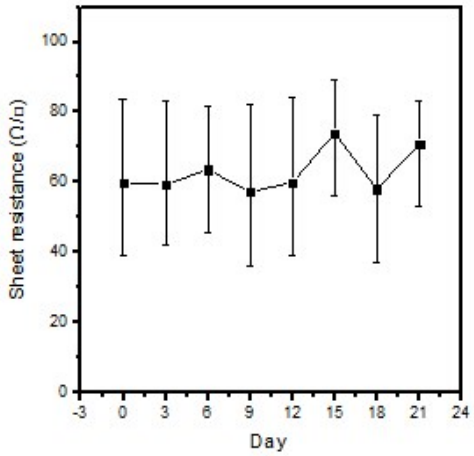

Fig. S18 The warm stability assessment of graphene-based E-textiles under 60 °C for various time durations.

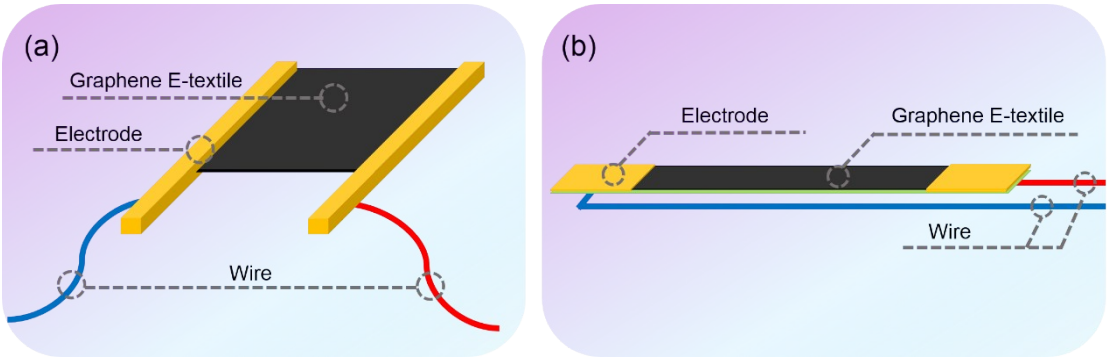

Fig. S19 (a) Schematic diagram of the pressure sensor and strain sensor. (b) Schematic diagram of a bending sensor.

Table S1. Comparison of the sensitivity, detection limit, and response time of our wearable pressure sensor with that in the literature.

Active materials	Working mechanism	Pressure range	Sensitivity	Response time [ms]	Wearable condition	Ref.
Silver NWs	Positive resistance type	13 Pa to 50 kPa	1.14 kPa^{-1}	≈17	Non-breathable, not washable	1
Au-coated PDMS micropillar/polyaniline	Positive resistance type	15 Pa to 3.5 kPa	2.0 kPa^{-1} below 0.22 kPa, 0.87 kPa^{-1} at 0.22–1.0 kPa	≈50	Non-breathable, not washable	2
SWCNT film/micropatterned PDMS	Positive resistance type	0.6 Pa to 1.2 kPa	1.8 kPa^{-1} below 0.3 kPa	<10	Non-breathable, not washable	3
CNT–PDMS composite with microdome arrays	Positive resistance type	0.2 Pa to 59 kPa	15.1 kPa^{-1} below 0.5 kPa	40	Non-breathable, not washable	4
Hierarchically structured graphene	Positive resistance type	1 Pa to 12 kPa	8.5 kPa^{-1}	40	Non-breathable, not washable	5
Fingerprint-like 3D graphene film	Positive resistance type	0.2 Pa to 75 kPa	110 kPa^{-1} below 200 Pa, 3 kPa^{-1} at 0.2–15 kPa, 0.26 kPa^{-1} at 15–75 kPa	30	Non-breathable, not washable	6
CNT–graphene composite film	Positive resistance type	0.6 Pa to 6 kPa	19.8 kPa^{-1} below 0.3 kPa, 0.27 kPa^{-1} above 0.3 kPa	16.7	Non-breathable, not washable	7
rGO-coated PU foam	Positive resistance type	<10 kPa	0.26 kPa^{-1} below 2 kPa, 0.03 kPa^{-1} at 2–10 kPa	–	Non-breathable, not washable	8
CNT-coated textile/Ni-coated textile	Positive resistance type	6 Pa to 20 kPa	14.4 kPa^{-1} below 3.5 kPa, 7.8 kPa^{-1} at 3.5–15 kPa	≈24	Non-breathable, not washable	9
3D carbonized cotton sponge	Positive resistance type	<700 kPa	Maximum 6.04 kPa^{-1}	–	Non-breathable, not washable	10
Carbonized silk nanofiber membrane	Positive resistance type	0.8 Pa to 5 kPa	34.47 kPa^{-1} at 0.8–400 Pa, 1.16 kPa^{-1} at 0.4–5 kPa	≈16.7	Non-breathable, not washable	11
Graphene E-textile	Positive resistance type	1.5 Pa to 17.5 kPa	Maximum 18.56 kPa^{-1}	23 ms	Breathable and washable	Our work

Table S2. Comparison of the performance of our wearable strain sensor with that in the literature.

Materials	Working mechanism	Strain range	Sensitivity [GF]	Wearable condition	RefM
Silver NWs	Negative resistance type	<70%	2–14, tunable	Non-breathable, not washable	12
Platinum NPs	Negative resistance type	<2%	16 000 at 2% strain	Non-breathable, not washable	13
Aligned SWCNT films	Negative resistance type	<280%	0.82, 0.06 within strain of 0–40%, 60–200%	Non-breathable, not washable	14
Thickness-gradient CNT film	Negative resistance type	<150%	161 within 2% strain; 9.8, 0.58 within strain of 2–15%, 15–150%	Non-breathable, not washable	15
Dry-spun CNT fiber	Negative resistance type	<960%	0.54 within 400% strain; 64 within strain of 400–960%	Non-breathable, not washable	16
CNT–PDMS composite	Negative resistance type	<120%	27.8, 1084, 9617 within strain of 0–40%, 40–90%, 90–120%	Non-breathable, not washable	17
Graphene mesh	Negative resistance type	<8%	500 within 2% strain; 10 000 at 8%	Non-breathable, not washable	18
Crumpled/wrinkled graphene film	Negative resistance type	<70%	0.76, 1.67, 2.55 at 10%, 40%, 70% strain	Non-breathable, not washable	19
rGO-based fiber	Negative resistance type	0.2–100%	10, 3.7 within 1%, 50% strain <100	Non-breathable, not washable	20
3D graphene foam/CNT composite	Negative resistance type	<85%	2.0, 20.5 at 5%, 85% strain	Non-breathable, not washable	21
Pencil-drawn graphite	Negative resistance type	-0.62%–0.62%	150.5, 60.6, 536.6 within strain of −0.62% to −0.32%, −0.22 to 0.22%, 0.32–0.62%	Non-breathable, not washable	22
Carbonized silk fabric	Negative resistance type	<500%	9.6 within 250% strain, 37.5 within strain of 250–500% <70	Non-breathable, not washable	23
Graphene/Polydimethylsiloxane	Negative resistance type	<20%	-	Non-breathable, not washable	24
Graphene and Carbon Nanotube	Negative resistance type	<20%	-	Non-breathable, not washable	25
Graphene Textile	Positive resistance type	<15%	−26 in the strain range of 8% under y-direction stretching and −1.7 in the strain range of 15% in the x-direction	Non-breathable, washable	26
Graphene E-textile	Positive resistance type	<22.5%	-14.26 (Maximum)	Breathable and washable	Our work

References

1 S. Gong, W. Schwalb, Y. Wang, Y. Chen, Y. Tang, J. Si, B. Shirinzadeh, W. Cheng, Nat. Commun. 5 (2014) 3132-3140.

2 H. Park, Y. R. Jeong, J. Yun, S. Y. Hong, S. Jin, S. J. Lee, G. Zi, J. S. Ha, ACS Nano 9 (2015) 9974-9985.

3 X. Wang, Y. Gu, Z. Xiong, Z. Cui, T. Zhang, Adv. Mater. 26 (2014) 1336-1342.

4 J. Park, Y. Lee, J. Hong, M. Ha, Y. D. Jung, H. Lim, S. Y. Kim, H. Ko, ACS Nano 8 (2014) 4689-4697.

5 G. Y. Bae, S. W. Pak, D. Kim, G. Lee, D. H. Kim, Y. Chung, K. Cho, Adv. Mater. 28 (2016) 5300-5306.

6 K. Xia, C. Wang, M. Jian, Q. Wang, Y. Zhang, Nano Res. 11 (2018) 1124-1134.

7 M. Jian, K. Xia, Q. Wang, Z. Yin, H. Wang, C. Wang, H. Xie, M. Zhang, Y. Zhang, Adv. Funct. Mater. 27 (2017) 1606066.

8 H. B. Yao, J. Ge, C. F. Wang, X. Wang, W. Hu, Z. J. Zheng, Y. Ni, S. H. Yu, Adv. Mater. 25 (2013) 6692-6698.

9 M. Liu, X. Pu, C. Jiang, T. Liu, X. Huang, L. Chen, C. Du, J. Sun, W. Hu, Z. L. Wang, Adv. Mater. 29 (2017) 1703700.

10 Y. Li, Y. A. Samad, K. Liao, J. Mater. Chem A 3 (2015) 2181-2187.

11 Q. Wang, M. Jian, C. Wang, Y. Zhang, Adv. Funct. Mater. 27 (2017) 1605657.

12 M. Amjadi, A. Pichitpajongkit, S. Lee, S. Ryu, I. Park, ACS Nano 8 (2014) 5154-5163.

13 B. Park, J. Kim, D. Kang, C. Jeong, K. S. Kim, J. U. Kim, P. J. Yoo, T. I. Kim, Adv. Mater. 28 (2016) 8130-8137.

14 T. Yamada, Y. Hayamizu, Y. Yamamoto, Y. Yomogida, A. Izadi-Najafabadi, D. N. Futaba, K. Hata, Nat. Nanotechnol. 6 (2011) 296.

15 Z. Liu, D. Qi, P. Guo, Y. Liu, B. Zhu, H. Yang, Y. Liu, B. Li, C. Zhang, J. Yu, Adv. Mater., 27 (2015) 6230-6237.

16 S. Ryu, P. Lee, J. B. Chou, R. Xu, R. Zhao, A. J. Hart, S. G. Kim, ACS Nano 9 (2015) 5929-5936.

17 J. Park, Y. Lee, J. Hong, Y. Lee, M. Ha, Y. Jung, H. Lim, S. Y. Kim, H. Ko, ACS Nano 8 (2014) 12020-12029.

18 Y. Wang, L. Wang, T. Yang, X. Li, X. Zang, M. Zhu, K. Wang, D. Wu, H. Zhu, Funct. Mater. 24 (2014) 4666-4670.

19 T. Yang, X. Jiang, Y. Zhong, X. Zhao, S. Lin, J. Li, X. Li, J. Xu, Z. Li, H. Zhu, ACS Sens. 2 (2017) 967-974.

20 Y. Cheng, R. Wang, J. Sun, L. Gao, Adv. Mater. 27 (2015) 7365-7371.

21 Q. Liu, J. Chen, Y. Li, G. Shi, ACS Nano 10 (2016) 7901-7906.

22 X. Liao, Q. Liao, X. Yan, Q. Liang, H. Si, M. Li, H. Wu, S. Cao, Y. Zhang, Adv. Funct. Mater. 25 (2015) 2395-2401.

23 C. Wang, X. Li, E. Gao, M. Jian, K. Xia, Q. Wang, Z. Xu, T. Ren, Y. Zhang, Adv. Mater. 28 (2016) 6640-6648.

24 Z. Wang, W. Gao, Q. Zhang, K. Zheng, J. Xu, W. Xu, E. Shang, J. Jiang, J. Zhang, Y. Liu, ACS Appl. Mater. Interfaces 11 (2018) 1344-1352.

25 J. Shi, X. Li, H. Cheng, Z. Liu, L. Zhao, T. Yang, Z. Dai, Z. Cheng, E. Shi, L. Yang, Z. Zhang, A. Cao, H. Zhu, Y. Fang, Adv. Funct. Mater. 26 (2016) 2078-2084.

26 Z. Yang, Y. Pang, X. l. Han, Y. Yang, J. Ling, M. Jian, Y. Zhang, Y. Yang, T. L. Ren, ACS Nano 12 (2018) 9134-9141.